Design for Fast Optogenetic Screen In Mammalian Cells For Next Gen Ca^{2+} Sensors

Merrilee Thomas[1*], Scott Martinka[2], and Thom Hughes[1,2]

[1] Department of Neuroscience and Cell biology, Montana State University, Bozeman, Montana, United States of America

[2] Montana Molecular, Bozeman, Montana, United States of America

*Corresponding Author

Merrileethomas1@gmail.com

Abstract

Genetically encoded fluorescent biosensors are proving to be powerful tools in neuroscience. The GCaMP6 Ca^{2+} sensor is widely used, and there are now many proof-of-principle versions for many second messengers that show promise. Improving these has been challenging because testing them involves a low throughput, labor-intensive processes. Our goal was to create a live cell system that uses a simple, reproducible, optogenetic process for testing prototypes of genetically encoded biosensors.

Blue light was used to activate an adenylyl cyclase enzyme from the soil bacterium *Beggiatoia* (bPAC) that increases intracellular cAMP (Stierl et al. 2011) as detected by the red sensor R-CaDDis. In turn the cAMP opened a cAMP gated channel (olfactory cyclic nucleotide gated channel, CNG, or the hyperpolarization-activated cyclic nucleotide gated channel, HCN2). This produced slow Ca^{2+} transients as detected by R-GECO1.2. To speed these transients up, we added the inwardly rectifying potassium channel 2.1, Kir2.1, and the bacterial voltage gated sodium channel (NAVROSD). This is a modular system in which the kinds of channels, and their relative amounts, can be tuned to produce the cellular behavior crucial for screening a particular biosensor in an automated format.

Introduction

Why are Ca^{2+} sensors important?

The calcium ion is an important second messenger in cellular processes ranging from neuronal function and muscle contractility, to fertilization and embryogenesis (Bear, Connors,

36 and Paradiso 2007). In the mammalian neuron, Ca^{2+} plays a role in many signaling pathways,
37 ultimately controlling the release of neurotransmitters from neurons. Genetically encoded Ca^{2+}
38 indicators contain fluorescent proteins that change fluorescence intensity as a function of Ca^{2+}
39 concentration (Kerruth et al. 2019; Huang et al. 2019) . They are minimally invasive, and since
40 they are genetically encoded their expression can be exquisitely targeted to specific cell types
41 and tissues (Agetsuma, Matsuda, and Nagai 2017; Bruton, Cheng, and Westerblad 2020; Kim
42 et al. 2019). The fluorescence of these biosensors is typically captured with wide field
43 microscopy and standard CCD cameras. However, there are many new imaging approaches
44 to capture the wealth of information they provide. Two photon microscopes make it possible to
45 image micro domains of Ca^{2+} signals within neurons in thick living tissue (T.-W. Chen et al.
46 2013; Peron et al. 2015). Light sheet microscopy makes it possible to now capture entire larval
47 zebrafish brain activity at single cell resolution at 2 Hz (Ahrens et al. 2013). Recently, Ca^{2+}
48 sensors are being coupled with functional magnetic resonance imaging (fMRI) (Barandov et al.
49 2019; Ghosh et al. 2018).

50 There are now several Ca^{2+} sensors that can sense Ca^{2+} transients in cells with
51 millisecond response times and that are bright enough to image in living tissue (Ouzounov et
52 al. 2017). Most of these sensors have blue excitation and green emission peaks. Currently, the
53 sensors with the fastest kinetic response time to Ca^{2+} flux are the Ultrafast GCaMP6f, jRCaMP
54 and jRGECO1a (Helassa et al. 2016; Kerruth et al. 2019). The recent jGCaMP7 sensor makes
55 it possible to capture individual action potentials and can track large neuronal populations
56 when using two photon or wide field imaging (Dana et al. 2019).

57 There is still a need for better Ca^{2+} sensors that are red (Zhao et al. 2011), or near IR
58 (Qian et al. 2019), because these longer wavelengths enable investigators to image deeper

into thick tissues that absorb and scatter light in the blue - green range. A greater maximal change in fluorescence for these sensors is needed, since a better signal to noise ratio can help increase imaging speeds and increase the field of view. Brighter sensors can be detectable with lower expression levels. This could be important since overexpression can lead to epileptiform activity (Dana et al. 2019). Sensors built with calcium binding properties such as calmodulin present specific problems *in vivo* such as buffering the internal Ca^{2+} concentration, and activation of kinases and phosphatases, and modulate ion channels(Mank and Griesbeck 2008). Further, creating sensors with linear response functions is needed, since the nonlinearities in GCaMP has led to decreased ability to accurately detect spikes (Deneux et al. 2016). Finally, jGCaMP7 and G-GECO1 sensors are imaged using green light. The short wavelengths of light needed to image these sensors can heat and damage the brain, which decreases the duration of imaging possible of the tissue (Podgorski and Ranganathan 2016).

One of the most effective approaches to expanding the fluorescent biosensor toolbox involves screening thousands of prototypes and then evolving for optimal function(Ibraheem et al. 2011; Park et al. 2013; Ding et al. 2015; Alford et al. 2012). For ease of use, this can be done in *E.coli*. colonies or lysates where it is possible to screen >10,000 colonies per round of evolution (Zhao et al. 2011); (Zhao et al. 2014). A drawback of this approach is that a sensor that works in *E.coli* may not work as well in mammalian cells. A more labor intensive, lower throughput, approach is to screen in mammalian neurons. For example, in the evolution of GCaMP6 to GCaMP7, 446 variants were screened, similarly R-Geco to J-RGeco1 required screening 689 variants, and RCaMP1 to JRCaMP1 screened 934 variants (Dana et al. 2016, 2019).

What if we could screen thousands of variants in mammalian cells for sensitivity, speed and dynamic range? In theory Ca^{2+} sensors could be screened in excitable human embryonic kidney cells (HEK-293 cells). The Cohen lab has pioneered the use of excitable HEK-293 cells to screen voltage sensors. They combined the inwardly rectifying potassium channel (Kir2.1) and voltage gated sodium channel (NAV1.3) and field stimulation to produce rhythmic depolarization and hyperpolarization in HEK cells (Park et al. 2013; Zhang, Reichert, and Cohen 2016),(Shah et al. 2004). They then created a stable cell line that expresses Kir2.1, Nav1.7 and CheRiff, a channelrhodopsin. This can be photoactivated thereby creating a system that produced oscillating membrane voltage (Zhang and Cohen 2017). Yet, there are inherent problems with stable cell lines, such as drift and silencing. In addition, the level of expression of each of the channels cannot be easily changed.

Similarly, another paper described a cell line that had pacemaker like activity. They stably expressed the HCN2 and Kir2.1 channels, and transiently expressed a voltage-gated channel Cav3.1 or Nav5.1 (K. Chen et al. 2018). HCN2 is a hyperpolarization activated, cyclic nucleotide gated ion channel (K. Chen et al. 2018). Nav1.5 is a voltage gated sodium channel responsible for action potentials in cardiomyocytes (K. Chen et al. 2018). Chen et al. found that cells expressing HCN2 and Kir2.1 had action potentials with depolarizations that last over ~450 ms, and a hyperpolarization phase that lasts ~737 ms (K. Chen et al. 2018). With either Cav3.1 or Nav5.1 expressed in conjunction with the Kir2.1 and HCN2, they found that there was an average of one action potential per second. This suggests that even without field stimulation, cells expressing these channels can create their own auto-depolarization leading to rhythmic oscillations in membrane potential. They also showed that the currents produced by the voltage gated channels influenced the speed at which the action potentials occur.

104 In theory, we could use similar channels to create cells that do not require field
105 stimulation, and have faster action potentials and whole cell Ca^{2+} transients. We wanted the
106 system to be automatable, inexpensive, modular, and useful in many different cell types. Our
107 goal was to create a screening platform for biosensors that is consistent, reliable, and capable
108 of quickly screening thousands of prototypes.

109 Results

110 Establishing an Optical Actuator

111 How can we actuate a biosynthetic cell line using light? To develop a optogenetically
112 controlled screen we chose to use bPAC (blue photo activated cyclase), a blue light activated
113 adenylyl cyclase from the soil bacteria *Beggiatoia* (Stierl et al. 2011). bPAC enzyme is
114 activated with 480 nm light which then converts ATP into cyclic adenosine monophosphate
115 (cAMP). R-caDDis is a fluorescent cAMP sensor that is excited with 561 nm light (Bernal
116 Sierra et al. 2018). We began by examining whether blue light stimulus can produce a
117 measurable change in cAMP levels in HEK-293 cells.

118 We transduced HEK-293 cells with bPAC (2x10^11 Vg/mL, viral titer) and R-caDDis (5 x
119 10^10 Vg/mL) (Fig.1 A). The following day the cells were stimulated with 10 milliseconds of
120 blue light and then images were collected continuously with 561 nm excitation that does not
121 activate bPAC. Upon blue light photoactivation, the R-CaDDis red fluorescence increased.
122 The quantification of the red fluorescence reveals that cAMP levels within the cell rise over the
123 time frame of ~100 seconds (Fig.1C). An obvious increase in red fluorescence can be seen
124 upon blue light activation and is demonstrated in the images of HEK-293 cells taken pre and

125 10 seconds post blue light stimulation (Fig.1B). Control cells with no bPAC did not show an
126 increase in red fluorescence. The system response is remarkably reproducible and the same
127 cells can be repeatedly stimulated. Indeed the only limitation is that too much blue light given
128 over a short period of time will create too much cAMP and saturate the sensor. The slow
129 decrease in fluorescence of R-CaDDis is most likely due to the phosphodiesterases present in
130 the cell which work to eliminate cAMP (Tewson et al. 2016).

131 **Figure 1** : **20ms of blue light is sufficient to activate bPAC.** A) HEK-293 cells were
132 transduced with bPAC (the actuator) and red-caDDis, the red fluorescence cAMP sensor. B)
133 The cells were briefly illuminated with 20ms of 480nm light. This activation of bPAC increases
134 cAMP levels which increases R-cADDis fluorescence. Brightness and contrast were the same
135 for both images. C) 20 ms of blue light activates bPAC which produces bursts of cAMP over a
136 period of 100 seconds. This is a stereotyped response that is repeatable with multiple doses of
137 blue light.

138 Dose Dependence

139 To examine the dose-response relationship for blue light and cAMP production, the
140 intensity of the blue light was systematically varied during stimulation while quantifying the r-
141 CaDDis fluorescence. HEK-293 cells were transduced with bPAC and R-caDDis, and each
142 well in a 96-well plate was given a 15 milliseconds dose of blue light. For each well, the power
143 of the LED 480nm light was increased stepwise from 0% to 100% in increments of five using a
144 THORLABS LED controller. At 100% power the light source measured 70mW/cm^2. Figure 2
145 reveals a near-linear dose response in which increasing levels of blue light produces increases
146 in cAMP levels. Above 50% power to the LED, there was an increased variability in the

147 response that is most likely due to saturating the sensor with cAMP. It is possible that lowering
148 the level of bPAC expression would make it possible to create a system with a greater range of
149 tunability before saturating the sensor with cAMP. The fluorescence change, delta F, was used
150 to determine the cAMP level and all points in the dose response are an average of multiple
151 trials (Fig. 2).

152 **Figure 2**: **There is a linear dose/response relationship between the power of blue**
153 **excitation and the fluorescence response of R-caDDis.** As the blue light intensity
154 increases so does the cAMP production. The delta F is a measure between the base and max
155 of the change in fluorescence (inset). Each data point represents an average of four trials.

156 Coupling the Actuator with an ion Channel

157 To couple cAMP production with depolarization, we expressed a cyclic nucleotide-gated
158 ion (CNG or HCN2) channel. The CNG channel is normally gated by cyclic guanosine
159 monophosphate (cGMP) (Fesenko, Kolesnikov, and Lyubarsky 1985). However, several
160 mutations can be introduced (Rich et al. 2000) that render it sensitive to cAMP. In theory, this
161 mutant channel should couple bPAC activation to a current that depolarizes the cell. In addition
162 the HCN2 is cAMP gated and must be hyperpolarized to activate(K. Chen et al. 2018).

163 We expressed a CNG channel (1.26 x 10^11 Vg/mL), bPAC, and R-GECO1 in HEK
164 cells (Fig. 3A). We triggered the activation of bPAC with blue light. Figure three illustrates that
165 upon 20ms of blue light activation of the enzyme, the red fluorescence of R-GECO increased.
166 The opening of the CNG channel increased Ca^{2+} levels in the cell which was quantified by an
167 increase in red fluorescence levels of R-GECO1 [16] (Fig. 3). The Ca^{2+} levels (Fig 3. B) stayed

168 elevated for ~30-80 seconds before their levels began to fall. The control cells without bPAC
169 showed no response (supplemental Fig. 2).

170 **Figure 3: Activation of bPAC leads to a Ca^{2+} transient when CNG or HCN2 is**
171 **expressed.** A) Blue light stimulation of bPAC should produce cAMP that inturn opens the
172 mutant CNG channel. B) The red trace is the R-GECO response to 20 ms of blue light
173 activation in cells with both the CNG and bPAC. C) Blue light stimulation of bPAC should
174 produce cAMP that opens the HCN2 channel. D) the trace is the R-GECO1 response to 20ms
175 of blue light activation in cells with both the HCN2 and bPAC.

176 Additional Channels Can Tune the Speed and Frequency of Ca^{2+} Transients

177 While the bPAC and CNG or HCN2 produced very reliable Ca^{2+} transients, these were
178 long lived events with slow kinetics. In theory introducing voltage regulated potassium and
179 sodium conductance could speed these transients up. The recent paper by Chen et al. found
180 that varying the levels of Kir2.1, and Cav1.3 or Nav1.5 affected the membrane oscillations
181 when recording membrane voltage using electrophysiology (K. Chen et al. 2018).

182 Wild type HEK-293 cells have a resting membrane potential of -25 mV but with Kir2.1
183 expressed their resting potential decreases to -70mV (Nguyen, Kirkton, and Bursac 2016;
184 Hille 2001; Kirkton and Bursac 2011; Yu et al. 2004). Kir2.1 is an inwardly rectifying potassium
185 channel that upon hyperpolarization greater than -20mV increases its conductance producing
186 an outward current (Hille 2001).

187 A 2016 study by the Bursac lab (Nguyen, Kirkton, and Bursac 2016) describes the
188 bacterial sodium channel, NavRosDg217a (NavD). It is characterized by a rapid activation
189 state that begins to open when the cell depolarizes to -30mV and a slow inactivation state

190 (hundreds of milliseconds) that starts during the depolarization (Nguyen, Kirkton, and Bursac
191 2016). The NavD channel is rapidly inactivated at +40mV, although, it must return to a
192 hyperpolarized state below -40mV for it to move from an inactivated state to deactivated, at
193 which point the channel can re-open (Nguyen, Kirkton, and Bursac 2016). Co-expressing the
194 NavD channel with Kir2.1 can create an excitable system because the Kir2.1 hyperpolarizes
195 the cell after each spontaneous depolarization of the sodium channel.

196 We choose the NavRosDg217A for two reasons. First, the human sodium channel has
197 an enormous coding region that exceeds the carrying capacity of most viruses. Bacterial
198 channel subunits are much smaller. Secondly, we wanted to create a system with long slow
199 depolarizations such that membrane depolarization events could be captured with slower
200 imaging speeds (10Hz). We transduced the bacterial channel NavRosDg217A (Nguyen,
201 Kirkton, and Bursac 2016), Kir2.1, CNG, and R-GECO1 into HEK-293 cells. There is some
202 degree of spontaneous activity, but when we activate bPAC with 20ms of blue light there were
203 robust responses in all of the wells. There were obvious Ca^{2+} transients that occurred in 90%
204 of the cells, but the activity was largely uncoordinated. Each cell has its own "signature"
205 change in Ca^{2+} levels, as seen in the R-GECO1 fluorescence traces (Fig.4B). The
206 fluorescence traces encode the change in the intracellular Ca^{2+} concentration levels of the cell.

207 **Figure 4: The kir2.1 and voltage gated sodium channel is vital for creating faster**
208 **Ca^{2+} transients.** A) In theory introducing the NavD and Kir2.1 channel should create faster
209 oscillating Ca^{2+} transients in the cell. B) Each cell has a unique Ca^{2+} transient response after
210 blue light stimulation of bPAC.

211 ## Optimizing the Activity

212 Our goal was to create a highly reproducible system that can be optimized. We propose
213 that different levels of the Kir2.1 and NavD would lead to varying responses. We systematically
214 transduced cells with varying ratios of Kir2.1 and NavD while holding the levels of bPAC and
215 CNG channels constant. The different ratios of the channels lead to different responses. To
216 quantify the Ca^{2+} imaging data we analyzed data using a custom made Matlab Program (Fig.
217 5A). We wanted to break down each Ca^{2+} transient into components that could be analyzed
218 and looked at in multiple ways. For each Ca^{2+} transient we examined the prominence of the
219 peak, the full width of the peak at half maximum (FWHM), and the inter-peak interval.
220

221 **Figure 5: Optimizing the ratios of voltage gated channels in the unstable system**
222 **illustrated in figure 4.** A) Diagram of the Matlab analysis of the Ca^{2+} transients. Peak
223 intensity, full width of the peak at half maximum (FWHM), and inter-peak intervals were
224 analyzed. B) Varying the ratios of Kir2.1 to NavD produce varying Ca^{2+} transient event widths.
225 The mean peak (FWHM) was analyzed with the standard deviation(SD) of the mean reported.
226 C) The mean intervals between peaks correlate with the varied levels of Kir2.1 to NavD. SD of
227 mean shown. D) Peak intensity histograms of Ca^{2+} transient events in cells transduced with a
228 Kir2.1 to NavD ratio of 14:1.

229 The Peak Finder in Matlab marks the peaks by their location in time and their maximum
230 fluorescence intensity. The peak intensity was then measured from the base fluorescence to
231 the peak that was pre-determined using the Matlab Peak Finder (Fig. 5A). The peak intensity
232 of the events does not appear to be random. Histograms of peak intensity (Fig. 5D) show what
233 appear to be units of activity as though the Ca^{2+} response is integrating one, two, or three
234 events.

235 In addition, we examined the width of the peak which was measured as the full width of
236 the peak at half maximum (Fig. 5A). The peak (FWHM) of the Ca^{2+} event is the length of time
237 that the Ca^{2+} concentration stayed elevated for each defined peak. The fastest event occurred
238 for 120ms, to ensure that each event was captured we sampled with continuous 40ms
239 exposures. The fastest average event (Peak FWHM) for a Ca^{2+} transient occurred in cells with
240 a Kir2.1 to NavRosD viral infectious unit ratio of 22:1 and generally lasted for ~400ms. Next,
241 we measured the inter-peak interval, which is the difference between two consecutive peaks.
242 The inter-peak interval is a measure of how frequently Ca^{2+} transients occur in a given system
243 after a previous response. Again, the cells that exhibited the shortest average inter-peak
244 interval were cells that had the Kir2.1:NavD ratio of 22:1, although there was a great deal of
245 cell to cell variability. A single burst of blue light produced activity for an average of two- three
246 minutes.

247 Optimizing Activity with HCN2

248 The behavior of HCN2 was quite different than CNG. Figure six depicts the
249 experimental setup, with R-GECO1, bPAC, Kir2.1, and NavD introduced by viral transduction
250 followed by transient transfection of the HCN2 plasmid. The following day images were
251 collected with 561 nm excitation light for several minutes after a blue light activation pulse of
252 20ms.

253 **Figure 6: Replacing the CNG channel with the pacemaker HCN2 channel**
254 **increases the Ca^{2+} transient duration and the time between events.** A) The HCN2 channel
255 can be exchanged for CNG**.** B) The transient events lasted over several seconds. C) The

256 Inter-Peak Interval time increased in concordance to increased Ca^{2+} event widths. The
257 standard deviation of the mean is shown.

258 We found that the HCN2 produced longer inter-peak intervals, and longer Ca^{2+}
259 transients, than cells expressing the CNG channel (Fig. 6). We found that the fastest events
260 occurred in cells with a viral unit ratio of Kir2.1 to NavD of 14:1 with an average of ~3 seconds
261 (Fig.6b). Compared to cells expressing CNG, the HCN2 cells in general had Ca^{2+} transients
262 that lasted around seven seconds with the time between transients ranging between 30 to 60
263 seconds. Importantly, the HCN2 cells show continued Ca^{2+} transients that lasted for up to 14
264 minutes after a single stimulus of blue light.

265 Screening Green Sensors Is Possible

266 Although there are several well engineered Ca^{2+} biosensors that are green, there
267 is still room for improvement, and continued engineering on green Ca^{2+} sensors persists.
268 Further, if it is possible to image both red and green Ca^{2+} sensors simultaneously, that can be
269 used to benchmark the other in terms of speed, signal amplitude, and linearity. G-GECO1 is
270 based on the GCaMP sensor and is based on the circularly permuted GFP with a fusion to the
271 M13 and calmodulin at the N and C termini (Zhao et al. 2011). It is pH-sensitive and is
272 relatively dim until it is excited, at which point it has a two fold increase in fluorescence
273 compared to GCaMP3 (Zhao et al. 2011).

274 Imaging G-GECO while continuously activating bPAC was generally straightforward.
275 We held the virus amount of Kir2.1 at $4x10^{\wedge 14}$ VG/μL , and NavD at $1.7x10^{\wedge 13}$ VG/μL, at a viral
276 ratio of Kir2.1:NavD at 22:1. The CNG channel viral titer was held at $2.5x10^{\wedge 14}$VG/μL and we
277 expressed G-GECO1 heterologously (Fig. 7A). We varied the viral titer of bPAC from .5 - 4 x

$10^{\wedge 16}$ VG/μL . We found that decreasing the bPAC dilution to 1 x $10^{\wedge 16}$ VG/μL decreased the width of the Ca^{2+} event, as well as decreased the time between events (Supplemental Fig.1). In principal an image splitter could be used to compare red sensors of unknown speed with a benchmarked green sensor. This experiment shows that the system can be continuously activated using very low power light.

Figure 7: Green Ca^{2+} indicators can be screened with low levels of blue light. A) The continuous blue light illumination needed to image green Ca^{2+} sensors should continuously activate bPAC. However, by reducing the amount of bPAC expression we are able to create an unstable system. The viral titer ratio of Kir2.1:NavD are held constant (22:1) and the total viral amount of bPAC was systematically varied. B) Increased viral levels of bPAC lead to Ca^{2+} transients with longer widths. C) Increasing bPAC expression lead to increased time between events. Standard deviation of the mean is shown.

Discussion

Our goal was to create a simple, modular, reproducible system to screen Ca^{2+} sensors. The system can be optimized by varying the ratio of Kir2.1 to NavD channels, thereby changing the type of Ca^{2+} transients that occur and the frequency at which they occur. Therefore, optimizing the ratio of the channels to the experimenters preference for cell type and sensor can empower an automated screen for Ca^{2+} sensors with different dynamic properties.

The designing of the high throughput screen for Ca^{2+} sensors can be modified. If a slow sensor is preferable, the HCN2 channel with a greater Kir2.1 to NavD ratio is desirable. Otherwise, to discover a fast sensor with increased linearity to Ca^{2+} dynamics, the CNG

300 channel with a fast sodium channel would be favorable. For example, the Ca^{2+} transients width
301 (length of time transient occurs) could potentially be greatly reduced by using a faster voltage
302 gated sodium channel. In addition, several papers have shown that including the connexin-43
303 protein increases the gap junction coupling of the HEK-293 cells (Nguyen, Kirkton, and Bursac
304 2016; Kirkton and Bursac 2011; Fahrenbach, Mejia-Alvarez, and Banach 2007). We did not
305 test how connexin-43 might affect this system but speculate that it could potentially stabilize
306 the activity between the cells allowing for more consistent oscillations. If the throughput needs
307 to be increased, the screening process could be broken into two steps. First, the screen could
308 use a HCN2 channel (Fig.6A) and the cells could be imaged slowly without creating large data
309 files. The best variants could then be screened in cells expressing the CNG channel and a fast
310 sodium channel. These prototypes will be expressed in cells that also express a benchmark
311 sensor such as GCAMP7f. Finally, the most promising variants would then be photo physically
312 characterized (Molina et al. 2019; Barnett, Hughes, and Drobizhev 2017).
313 The progress on improving Ca^{2+} and voltage sensors depends on the throughput
314 of the screen (Park et al. 2013; Rodriguez et al. 2017). For example, the improvement of the
315 voltage sensors has been very slow due to limitations in the throughput involved in whole cell
316 patch clamp fluorometry (Storace et al. 2016; Park et al. 2013). The system described here will
317 enable investigators to screen without drugs or field stimulation. Recording the activity in a well
318 for a minute would eliminate false negatives and result in a time budget of roughly 100 minutes
319 per 96 well plate. Alternatively, the FLIPR (Schroeder and Neagle 1996; Arkin et al. 2012)
320 would make it possible to simultaneously screen 384 well plates which would move this screen
321 into a high throughput realm.

Methods

Growth conditions for HEK-293 cells

A line of HEK-293 were cultured in DMEM, 10% FBS, and 1% Penicillin (100 U/mL). For experiments, HEK-293 cells were plated in 96 well plastic plates at 200µl per well (~3 x10^5 cells/mL).

Plasmids

The HCN2 plasmid was kindly donated by Joan Lemire at Tufts University from Dr. Michael Levin's lab. The NavRosDg217 was reverse translated using a human codon preferences and synthesized as a Gblock by IDT (Coralville, Iowa). The cyclic nucleotide gated olfactory channel (Rattus norvegicus) has the following mutations, delta61–90/C460W/E583M and was synthesized as a Gblock by IDT. The rat channel can be found on NCBI at NP_037060.1 (Rich et al. 2001). pGEMTEZ-Kir2.1 was a gift from Richard Axel, Joseph Gogos & Ron Yu (Addgene plasmid #32641 ; http://n2t.net/addgene:32641 ; RRID:Addgene_32641)(Yu et al. 2004).

Baculovirus

The following channels, Kir2.1, CNG, and NavRosDg217 were placed into a BacMam plasmid and used to create high titer baculovirus (Montana Molecular, Bozeman, MT). The virus titers were: Kir2.1 titer 1.58x10^11 VG/mL, bPAC titer 1.98 x 10^11 VG/mL, CNG titer 1.26x10^11VG/mL, and NavRosDg217 titer 1.73 x 10^10VG/mL. The following bio-sensors

were obtained from Montana Molecular: The R-CaDDis (titer 5.06x10^10 Vg/mL); R-GECO (1.32x10^10 Vg/mL); and G-GECO (4.48x10^10 Vg/mL).

Transduction

HEK-293 cells were prepared and transduced following manufacturer's recommended protocol (Montana Molecular). HEK-293 cells were plated in 96 well plastic plates at a mono confluent layer of (3 x 10^5 cells/mL) and were imaged two days following transduction. The cells were washed with Tyrode's solution once and then each well was filled with 100µl of Tyrode's solution.

Transfection of HCN2

24 hours post transduction the HEK-293 cells were grown to ~80% confluency in 96 well plates and transfected using Mirus Bio *Trans*IT®-293 transfection reagent using the manufacturer's recommendation. Cells were transfected with the HCN2 plasmid at 100ng/µl.

An ASI modular microscope

The experiments were conducted using wide field imaging on an ASI-XYZ stage fitted with a modular infinity microscope. The objective imaged onto the detector chip of a Hamamatsu ORCA-Flash 4.0 scientific-CMOS camera. The images were collected using either matlab scripts that controlled the camera, ASI stage, SH1-Thorlabs shutter, and ThorLabs DC4100 Four Channel-LED Driver, or by using µmanager (Edelstein et al. 2014). A custom illumination system was arranged. Briefly, a dichroic mirror (**XX**) was positioned at the entrance of the microscope to combine blue light LED illumination with yellow laser illumination. An SH1-Thorlabs shutter was used to create brief illumination from a blue

362 ThorLABS LED (488nm) for rapid stimulation of bPAC. At 100% the blue light illumination was
363 70mW/cm^2. The yellow illumination was provided with a Sapphire laser(561nm, 50mW,
364 Coherent). The laser beam was steered with two mirrors (arranged in a periscope) into an
365 entrance aperture of the ASI microscope. Before entering the microscope, the laser beam was
366 diffused with a 50^0 diffuser (ED1 C50 MD, Thorlabs) placed in the focus of an f = 20 mm
367 aspheric lens (ACL2520U, Thorlabs) that collimated the beam for further traveling into the
368 microscope. The illumination intensity at 100% of the laser power at the sample was
369 10mW/cm^2.

370 ### Analysis

371 Image data was stored in a Z-stack tiff file and loaded into the FIJI distribution of the
372 ImageJ software (Schindelin et al. 2012). The background fluorescence was corrected using
373 the photobleaching gui in FIJI. The cells were hand selected using a freehand ROI surrounding
374 the cell of interest. The average pixel value within the ROI for each frame was then loaded into
375 MatLab. Analysis was built in Matlab using the Find Peaks in the Signal Processing Toolbox.
376 The find peaks returns a vector with the local maxima (peaks) from the ROI trace data. In
377 addition, it returns the widths of the peak and the prominence of the peak. The inter-event
378 interval is the vector difference between each consecutive peak.

379 ## Acknowledgements

380 Science doesn't exist in a vacuum, and because of this I would like to thank the
381 following people: Paul Tewson for HEK-293 cells. Scott Martinka for making lots of great high
382 titer virus. Kevin Harlett for having a deep love of analyzing data. Rosana Molina. Kaspar
383 Podgorski, Steven Hoffman, Dr. Mark Owkes, and Jonathan King for Matlab wizardry. Huge

thanks to Joan Lemire at Tufts University for quick turnaround time and HCN2 plasmid. For Thom Hughes and his strong belief in his graduate students. The Thomas family.

References

Agetsuma, Masakazu, Tomoki Matsuda, and Takeharu Nagai. 2017. “Methods for Monitoring Signaling Molecules in Cellular Compartments.” *Cell Calcium* 64 (June): 12–19.

Ahrens, Misha B., Michael B. Orger, Drew N. Robson, Jennifer M. Li, and Philipp J. Keller. 2013. “Whole-Brain Functional Imaging at Cellular Resolution Using Light-Sheet Microscopy.” *Nature Methods* 10 (5): 413–20.

Alford, Spencer C., Ahmed S. Abdelfattah, Yidan Ding, and Robert E. Campbell. 2012. “A Fluorogenic Red Fluorescent Protein Heterodimer.” *Chemistry & Biology* 19 (3): 353–60.

Arkin, Michelle R., Patrick R. Connor, Renee Emkey, Kim E. Garbison, Beverly A. Heinz, Todd R. Wiernicki, Paul A. Johnston, Ramani A. Kandasamy, Nancy B. Rankl, and Sitta Sittampalam. 2012. “FLIPR^{TM} Assays for GPCR and Ion Channel Targets.” In *Assay Guidance Manual*, edited by G. Sitta Sittampalam, Abigail Grossman, Kyle Brimacombe, Michelle Arkin, Douglas Auld, Chris Austin, Jonathan Baell, et al. Bethesda (MD): Eli Lilly & Company and the National Center for AdvancingTranslational Sciences.

Barandov, Ali, Benjamin B. Bartelle, Catherine G. Williamson, Emily S. Loucks, Stephen J. Lippard, and Alan Jasanoff. 2019. “Sensing Intracellular Calcium Ions Using a Manganese-Based MRI Contrast Agent.” *Nature Communications* 10 (1): 897.

Barnett, Lauren M., Thomas E. Hughes, and Mikhail Drobizhev. 2017. “Deciphering the Molecular Mechanism Responsible for GCaMP6m’s Ca2+-Dependent Change in Fluorescence.” *PloS One* 12 (2): e0170934.

Bear, Mark F., Barry W. Connors, and Michael A. Paradiso. 2007. *Neuroscience*. Lippincott Williams & Wilkins.

Bernal Sierra, Yinth Andrea, Benjamin R. Rost, Martin Pofahl, António Miguel Fernandes, Ramona A. Kopton, Sylvain Moser, Dominik Holtkamp, et al. 2018. “Potassium Channel-Based Optogenetic Silencing.” *Nature Communications* 9 (1): 4611.

Bruton, Joseph, Arthur J. Cheng, and Håkan Westerblad. 2020. “Measuring Ca2+ in Living Cells.” *Advances in Experimental Medicine and Biology* 1131: 7–26.

Chen, Kuihao, Dongchuan Zuo, Sho-Ya Wang, and Haijun Chen. 2018. “Kir2 Inward Rectification-Controlled Precise and Dynamic Balances between Kir2 and HCN Currents Initiate Pacemaking Activity.” *FASEB Journal: Official Publication of the Federation of American Societies for Experimental Biology* 32 (6): 3047–57.

Chen, Tsai-Wen, Trevor J. Wardill, Yi Sun, Stefan R. Pulver, Sabine L. Renninger, Amy Baohan, Eric R. Schreiter, et al. 2013. “Ultrasensitive Fluorescent Proteins for Imaging Neuronal Activity.” *Nature* 499 (7458): 295–300.

Dana, Hod, Boaz Mohar, Yi Sun, Sujatha Narayan, Andrew Gordus, Jeremy P. Hasseman, Getahun Tsegaye, et al. 2016. “Sensitive Red Protein Calcium Indicators for Imaging Neural Activity.” *eLife* 5 (March). https://doi.org/10.7554/eLife.12727.

Dana, Hod, Yi Sun, Boaz Mohar, Brad K. Hulse, Aaron M. Kerlin, Jeremy P. Hasseman, Getahun Tsegaye, et al. 2019. “High-Performance Calcium Sensors for Imaging Activity in Neuronal Populations and Microcompartments.” *Nature Methods* 16 (7): 649–57.

Deneux, Thomas, Attila Kaszas, Gergely Szalay, Gergely Katona, Tamás Lakner, Amiram Grinvald, Balázs Rózsa, and Ivo Vanzetta. 2016. “Accurate Spike Estimation from Noisy

Calcium Signals for Ultrafast Three-Dimensional Imaging of Large Neuronal Populations in Vivo." *Nature Communications* 7 (July): 12190.

Ding, Yidan, Jiao Li, Jhon Ralph Enterina, Yi Shen, Issan Zhang, Paul H. Tewson, Gary C. H. Mo, et al. 2015. "Ratiometric Biosensors Based on Dimerization-Dependent Fluorescent Protein Exchange." *Nature Methods* 12 (3): 195–98.

Edelstein, Arthur D., Mark A. Tsuchida, Nenad Amodaj, Henry Pinkard, Ronald D. Vale, and Nico Stuurman. 2014. "Advanced Methods of Microscope Control Using μManager Software." *Journal of Biological Methods* 1 (2). https://doi.org/10.14440/jbm.2014.36.

Fahrenbach, John P., Rafael Mejia-Alvarez, and Kathrin Banach. 2007. "The Relevance of Non-Excitable Cells for Cardiac Pacemaker Function." *The Journal of Physiology* 585 (Pt 2): 565–78.

Fesenko, E. E., S. S. Kolesnikov, and A. L. Lyubarsky. 1985. "Induction by Cyclic GMP of Cationic Conductance in Plasma Membrane of Retinal Rod Outer Segment." *Nature* 313 (6000): 310–13.

Ghosh, Souparno, Peter Harvey, Jacob C. Simon, and Alan Jasanoff. 2018. "Probing the Brain with Molecular fMRI." *Current Opinion in Neurobiology* 50 (June): 201–10.

Helassa, Nordine, Borbala Podor, Alan Fine, and Katalin Török. 2016. "Design and Mechanistic Insight into Ultrafast Calcium Indicators for Monitoring Intracellular Calcium Dynamics." *Scientific Reports* 6 (December): 38276.

Hille, Bertil. 2001. *Ionic Channels of Excitable Membranes*. Sinauer.

Huang, Lawrence, Ulf Knoblich, Peter Ledochowitsch, Jérôme Lecoq, R. Clay Reid, Saskia E. J. de Vries, Michael A. Buice, et al. 2019. "Relationship between Spiking Activity and Simultaneously Recorded Fluorescence Signals in Transgenic Mice Expressing GCaMP6." *bioRxiv*. https://doi.org/10.1101/788802.

Ibraheem, Andreas, Hongkin Yap, Yidan Ding, and Robert E. Campbell. 2011. "A Bacteria Colony-Based Screen for Optimal Linker Combinations in Genetically Encoded Biosensors." *BMC Biotechnology* 11 (November): 105.

Kerruth, Silke, Catherine Coates, Céline D. Dürst, Thomas G. Oertner, and Katalin Török. 2019. "The Kinetic Mechanisms of Fast-Decay Red-Fluorescent Genetically Encoded Calcium Indicators." *The Journal of Biological Chemistry* 294 (11): 3934–46.

Kim, Douglas, Karel Svoboda, Loren Looger, and Eric Schreiter. 2019. Genetically encoded calcium indicators and methods of use. USPTO 20190153067:A1. *US Patent*, filed November 21, 2018, and issued May 23, 2019. https://patentimages.storage.googleapis.com/48/48/53/5bb27ffa25d100/US20190153067A1.pdf.

Kirkton, Robert D., and Nenad Bursac. 2011. "Engineering Biosynthetic Excitable Tissues from Unexcitable Cells for Electrophysiological and Cell Therapy Studies." *Nature Communications* 2: 300.

Mank, Marco, and Oliver Griesbeck. 2008. "Genetically Encoded Calcium Indicators." *Chemical Reviews* 108 (5): 1550–64.

Molina, Rosana S., Yong Qian, Jiahui Wu, Yi Shen, Robert E. Campbell, Mikhail Drobizhev, and Thomas E. Hughes. 2019. "Understanding the Fluorescence Change in Red Genetically Encoded Calcium Ion Indicators." *Biophysical Journal* 116 (10): 1873–86.

Nguyen, Hung X., Robert D. Kirkton, and Nenad Bursac. 2016. "Engineering Prokaryotic Channels for Control of Mammalian Tissue Excitability." *Nature Communications* 7 (October): 13132.

Ouzounov, Dimitre G., Tianyu Wang, Mengran Wang, Danielle D. Feng, Nicholas G. Horton, Jean C. Cruz-Hernández, Yu-Ting Cheng, et al. 2017. "In Vivo Three-Photon Imaging of Activity of GCaMP6-Labeled Neurons Deep in Intact Mouse Brain." *Nature Methods* 14 (4): 388–90.

Park, Jeehae, Christopher A. Werley, Veena Venkatachalam, Joel M. Kralj, Sulayman D. Dib-

Hajj, Stephen G. Waxman, and Adam E. Cohen. 2013. “Screening Fluorescent Voltage Indicators with Spontaneously Spiking HEK Cells.” *PloS One* 8 (12): e85221.

Peron, Simon P., Jeremy Freeman, Vijay Iyer, Caiying Guo, and Karel Svoboda. 2015. “A Cellular Resolution Map of Barrel Cortex Activity during Tactile Behavior.” *Neuron* 86 (3): 783–99.

Podgorski, Kaspar, and Gayathri Ranganathan. 2016. “Brain Heating Induced by near-Infrared Lasers during Multiphoton Microscopy.” *Journal of Neurophysiology* 116 (3): 1012–23.

Qian, Yong, Kiryl D. Piatkevich, Benedict Mc Larney, Ahmed S. Abdelfattah, Sohum Mehta, Mitchell H. Murdock, Sven Gottschalk, et al. 2019. “A Genetically Encoded near-Infrared Fluorescent Calcium Ion Indicator.” *Nature Methods* 16 (2): 171–74.

Rich, Thomas C., Kent A. Fagan, Hiroko Nakata, Jerome Schaack, Dermot M. F. Cooper, and Jeffrey W. Karpen. 2000. “Cyclic Nucleotide–Gated Channels Colocalize with Adenylyl Cyclase in Regions of Restricted Camp Diffusion.” *The Journal of General Physiology* 116 (2): 147–62.

Rich, Thomas C., Tonia E. Tse, Joyce G. Rohan, Jerome Schaack, and Jeffrey W. Karpen. 2001. “In Vivo Assessment of Local Phosphodiesterase Activity Using Tailored Cyclic Nucleotide–Gated Channels as Camp Sensors.” *The Journal of General Physiology* 118 (1): 63–78.

Rodriguez, Erik A., Robert E. Campbell, John Y. Lin, Michael Z. Lin, Atsushi Miyawaki, Amy E. Palmer, Xiaokun Shu, Jin Zhang, and Roger Y. Tsien. 2017. “The Growing and Glowing Toolbox of Fluorescent and Photoactive Proteins.” *Trends in Biochemical Sciences* 42 (2): 111–29.

Schindelin, Johannes, Ignacio Arganda-Carreras, Erwin Frise, Verena Kaynig, Mark Longair, Tobias Pietzsch, Stephan Preibisch, et al. 2012. “Fiji: An Open-Source Platform for Biological-Image Analysis.” *Nature Methods* 9 (7): 676–82.

Schroeder, Kirk S., and Brad D. Neagle. 1996. “FLIPR: A New Instrument for Accurate, High Throughput Optical Screening.” *Journal of Biomolecular Screening* 1 (2): 75–80.

Shah, Bhaval S., Anthony M. Rush, Shujun Liu, Lynda Tyrrell, Joel A. Black, Sulayman D. Dib-Hajj, and Stephen G. Waxman. 2004. “Contactin Associates with Sodium Channel Nav1.3 in Native Tissues and Increases Channel Density at the Cell Surface.” *The Journal of Neuroscience: The Official Journal of the Society for Neuroscience* 24 (33): 7387–99.

Stierl, Manuela, Patrick Stumpf, Daniel Udwari, Ronnie Gueta, Rolf Hagedorn, Aba Losi, Wolfgang Gärtner, et al. 2011. “Light Modulation of Cellular cAMP by a Small Bacterial Photoactivated Adenylyl Cyclase, bPAC, of the Soil Bacterium Beggiatoa.” *The Journal of Biological Chemistry* 286 (2): 1181–88.

Storace, Douglas, Masoud Sepehri Rad, Bokeum Kang, Lawrence B. Cohen, Thom Hughes, and Bradley J. Baker. 2016. “Toward Better Genetically Encoded Sensors of Membrane Potential.” *Trends in Neurosciences* 39 (5): 277–89.

Tewson, Paul H., Scott Martinka, Nathan C. Shaner, Thomas E. Hughes, and Anne Marie Quinn. 2016. “New DAG and cAMP Sensors Optimized for Live-Cell Assays in Automated Laboratories.” *Journal of Biomolecular Screening* 21 (3): 298–305.

Yu, C. Ron, Jennifer Power, Gilad Barnea, Sean O’Donnell, Hannah E. V. Brown, Joseph Osborne, Richard Axel, and Joseph A. Gogos. 2004. “Spontaneous Neural Activity Is Required for the Establishment and Maintenance of the Olfactory Sensory Map.” *Neuron* 42 (4): 553–66.

Zhang, Hongkang, and Adam E. Cohen. 2017. “Optogenetic Approaches to Drug Discovery in Neuroscience and Beyond.” *Trends in Biotechnology* 35 (7): 625–39.

Zhang, Hongkang, Elaine Reichert, and Adam E. Cohen. 2016. “Optical Electrophysiology for Probing Function and Pharmacology of Voltage-Gated Ion Channels.” *eLife* 5 (May). https://doi.org/10.7554/eLife.15202.

Zhao, Yongxin, Ahmed S. Abdelfattah, Yufeng Zhao, Araya Ruangkittisakul, Klaus Ballanyi,

Robert E. Campbell, and D. Jed Harrison. 2014. “Microfluidic Cell Sorter-Aided Directed Evolution of a Protein-Based Calcium Ion Indicator with an Inverted Fluorescent Response.” *Integrative Biology* 6 (7): 714–25.

Zhao, Yongxin, Satoko Araki, Jiahui Wu, Takayuki Teramoto, Yu-Fen Chang, Masahiro Nakano, Ahmed S. Abdelfattah, et al. 2011. “An Expanded Palette of Genetically Encoded Ca^{2+} Indicators.” *Science* 333 (6051): 1888–91.

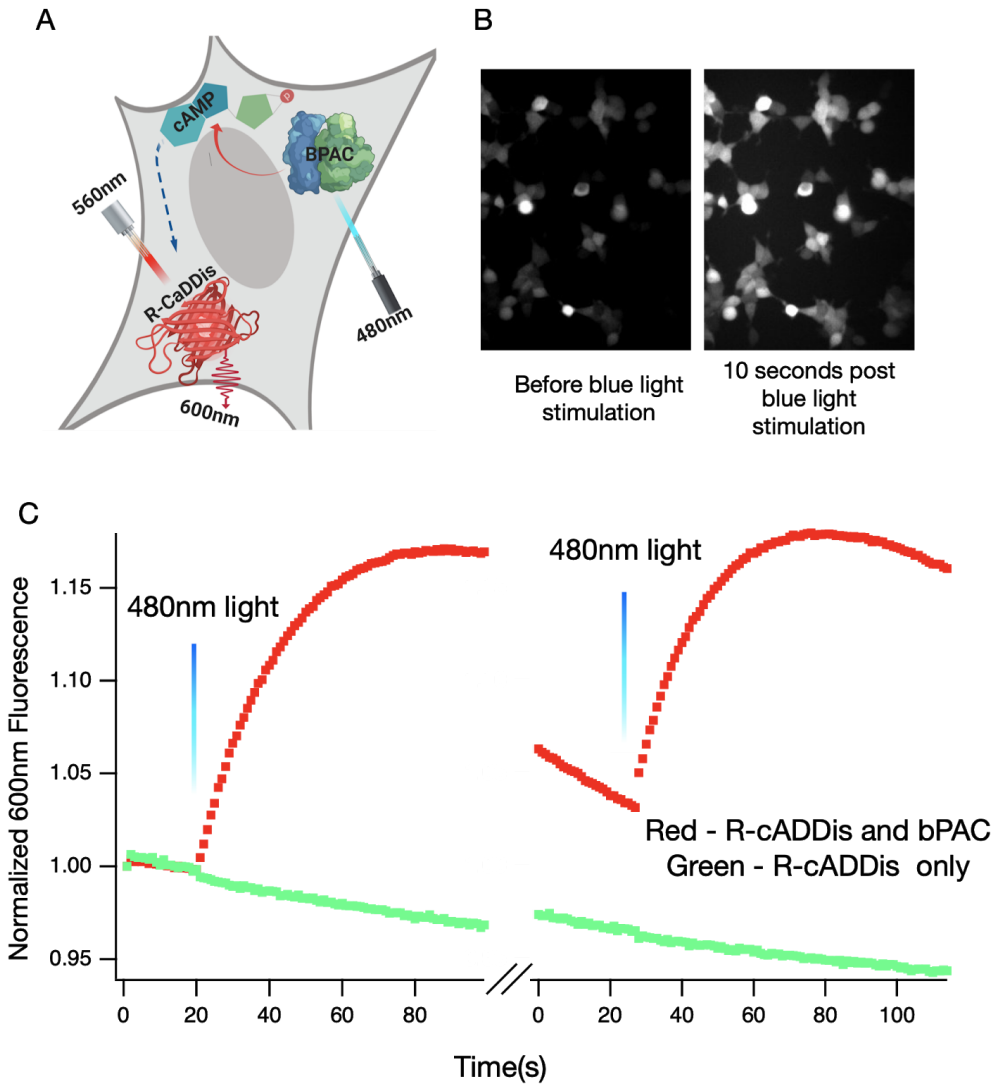

Figure one : Only 20ms of blue light is sufficient to activate bPAC. A) HEK-293 cells were transduced with bPAC (the actuator) and red-caDDis, the red fluorescence cAMP sensor. B) The cells were briefly illuminated with 20ms of 480nm light. This activation of bPAC increases cAMP levels which increases R-cADDis fluorescence. Brightness and contrast were the same for both images. C) 20 ms of blue light activates bPAC which produces bursts of cAMP over a period of 100 seconds. This is a stereotyped response that is repeatable with multiple doses of blue light.

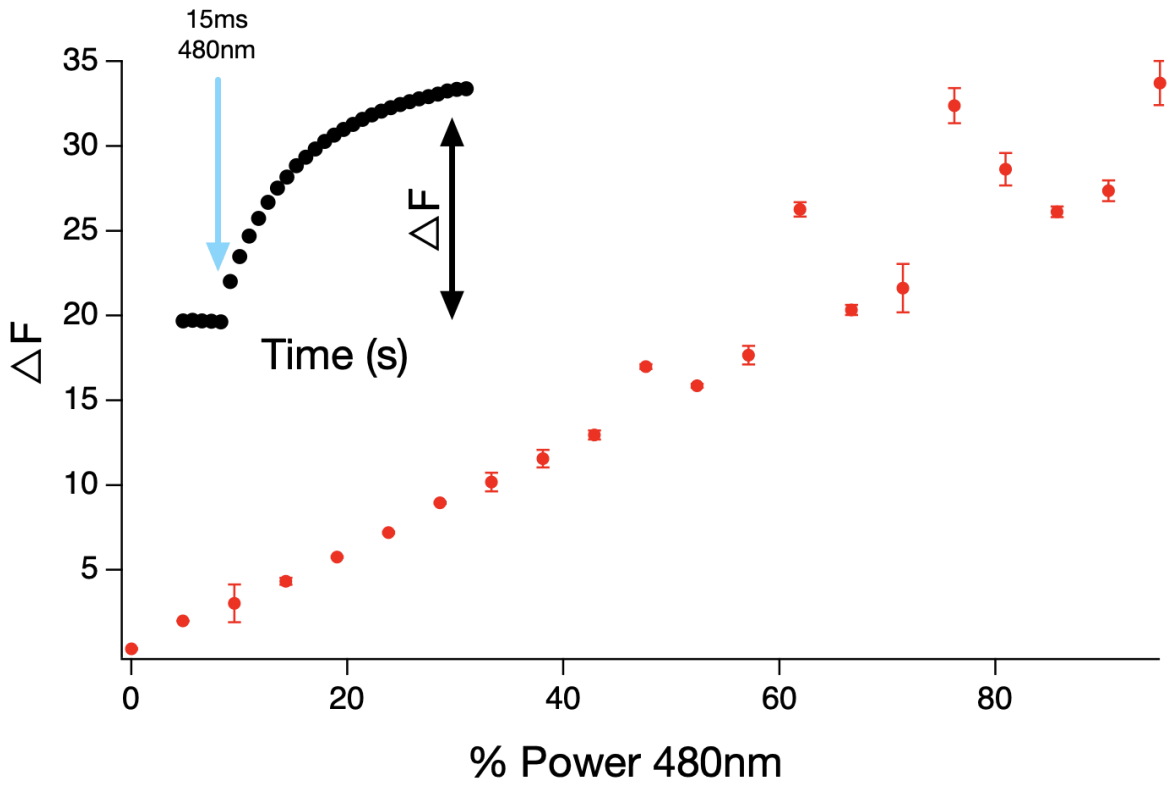

Figure 2: There is a linear dose/response relationship between the power of blue excitation and the fluorescence response of R-caDDis. As the blue light power increases so does the cAMP production. The delta F is a measure between the base and max of the change in fluorescence (inset). Each data point represents an average of multiple trials.

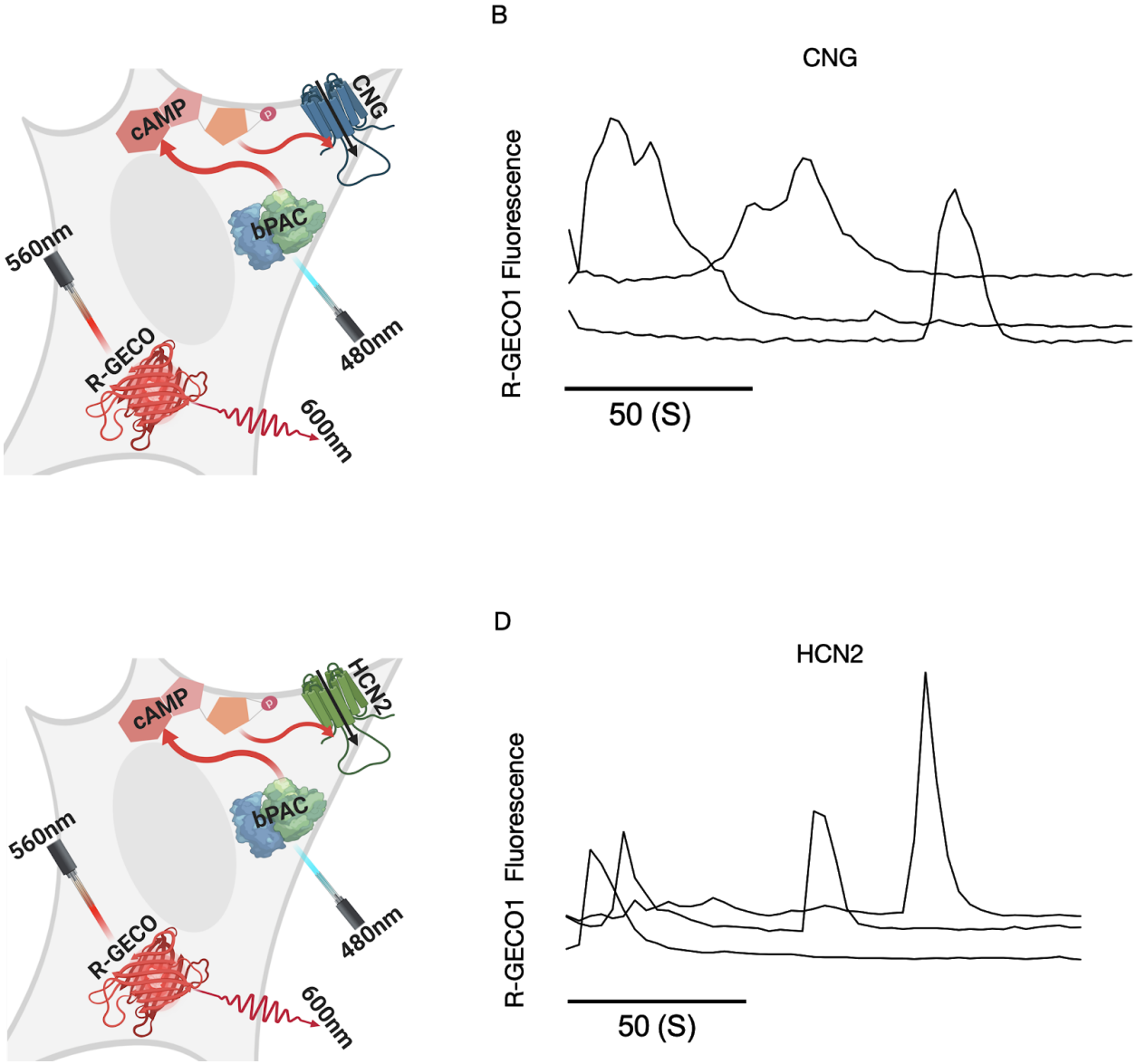

Figure 3: Activation of bPAC leads to a Ca2+ transient when CNG or HCN2 is expressed. A) Blue light stimulation of bPAC should produce cAMP that inturn opens the mutant CNG channel. B) The red trace is the R-GECO response to 20 ms of blue light activation in cells with both the CNG and bPAC. C) Blue light stimulation of bPAC should produce cAMP that opens the HCN2 channel. D) the trace is the R-GECO1 response to 20ms of blue light activation in cells with both the HCN2 and bPAC.

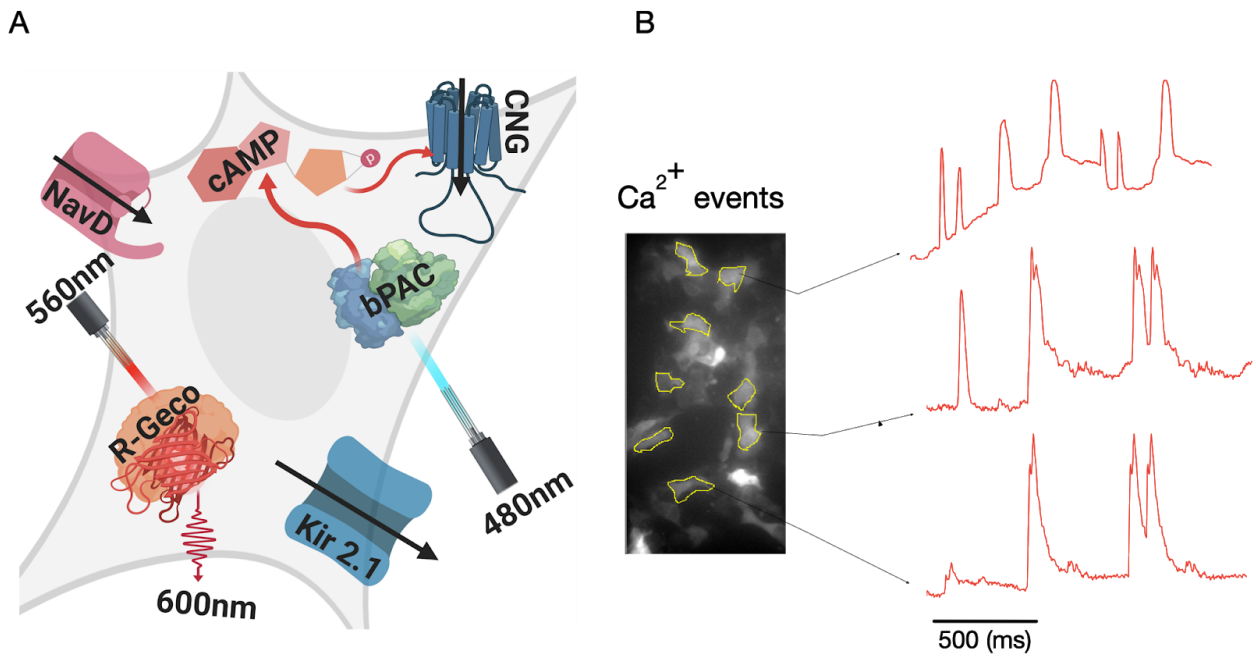

Figure Four : The voltage gated sodium channel is vital for creating an unstable system. A) In theory introducing the NavD channel should create oscillating calcium transients in the cell. B) Each cell has a unique calcium transient response after blue light stimulation of bPAC. C) A Z-projection of a time series shows the cumulative activity of cells over 60 seconds. Wells without bPAC show little to no activity.

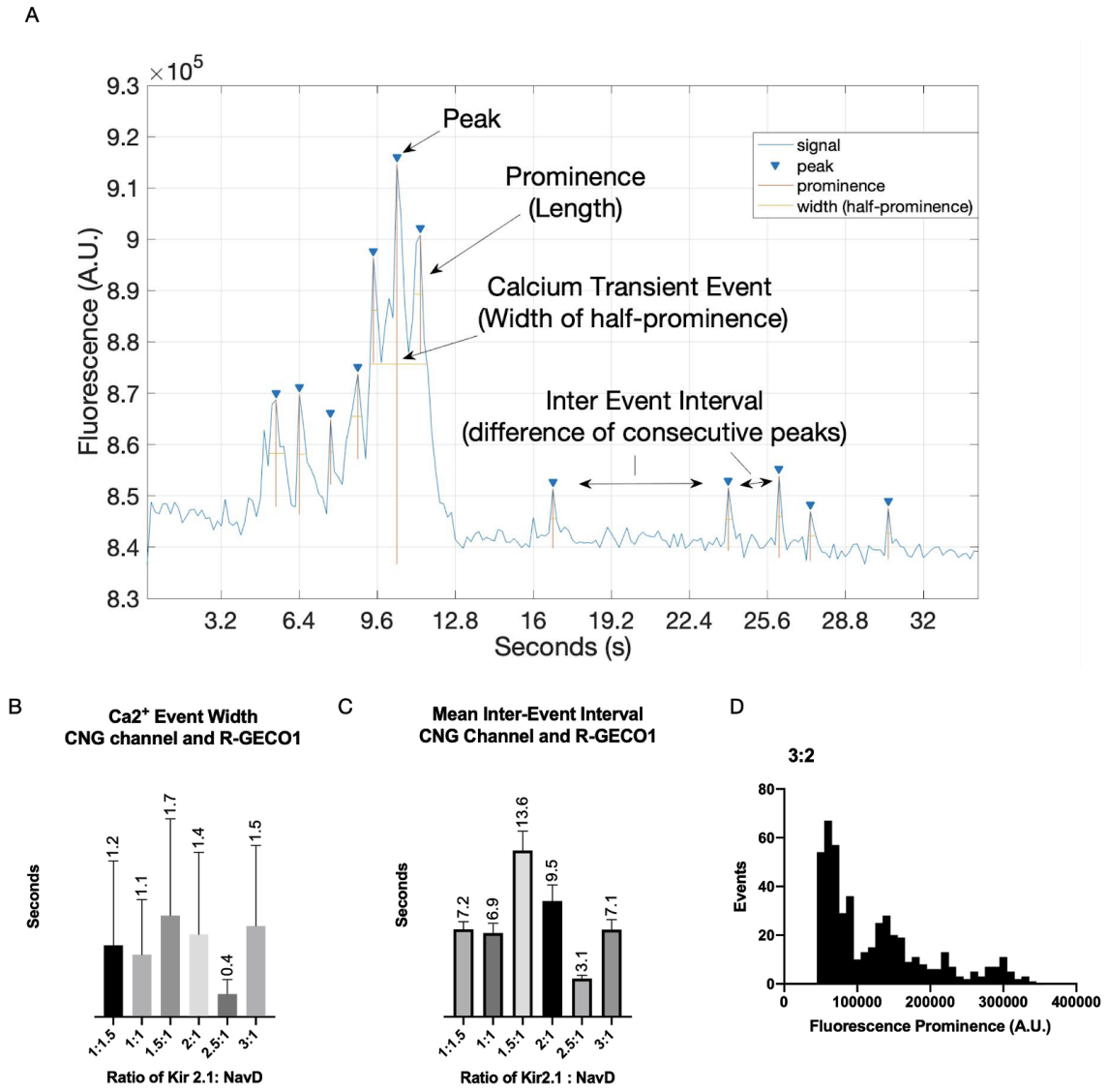

Figure 5: Optimizing the ratios of voltage gated channels in the unstable system illustrated in figure 4. A) Diagram of the Matlab analysis of the Ca^{2+} transients. Prominence, width of half prominence, and inter-event intervals were analyzed. B) Varying the ratios of Kir2.1 to NavD produce varying calcium transient event widths. C) The mean inter-event Interval changes in concordance to the varied levels of Kir to NavD. D) Prominence histogram of Ca^{2+} transient events in cells transduced with a 3:2 ratio of Kir to NavD.

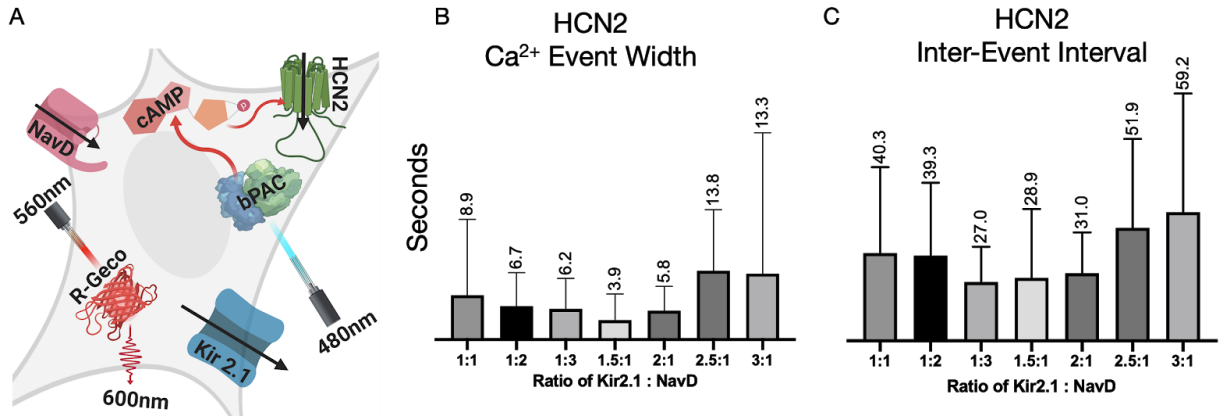

Figure 6: Replacing the CNG channel with the pacemaker HCN2 channel increases the Ca^{2+} transient duration and the time between events. A) The HCN2 channel can be exchanged for CNG**.** B) The transient events lasted over several seconds. C) The Inter-Event Interval time increased in concordance to increased calcium event widths.

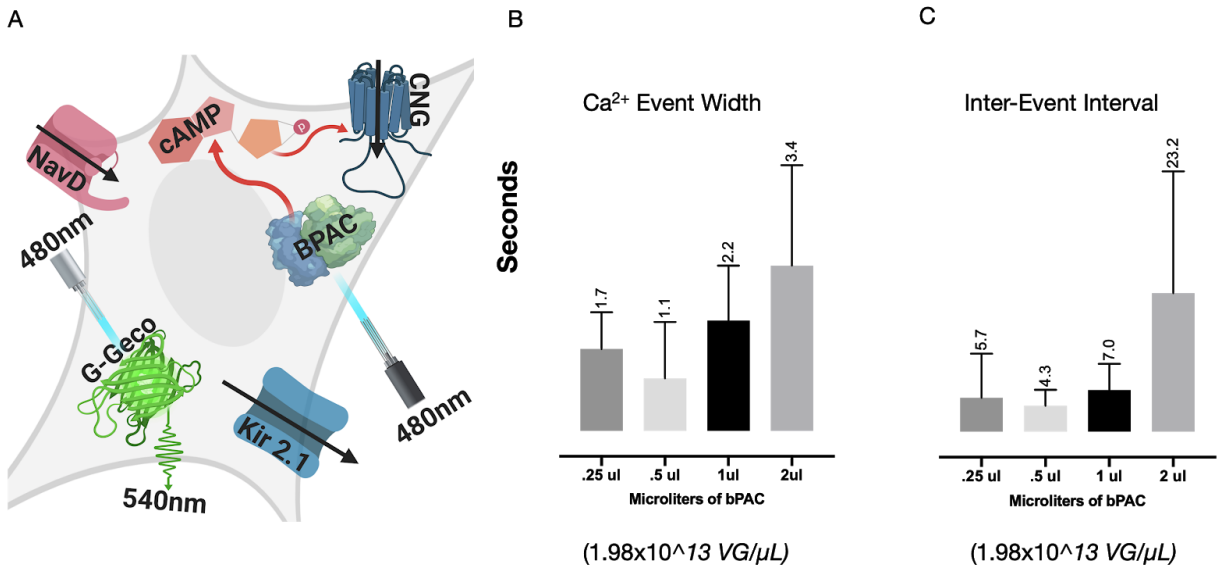

Figure Seven: Green Ca^{2+} indicators can screened with low levels of blue light. A) The continuous blue light illumination needed to image green Ca^{2+} sensors should continuously activate bPAC. However, by reducing the amount of bPAC expression we are able to create an unstable system. The levels of Kir:NavD are held constant (2.5:1) and the levels of bPAC were systematically varied. B) Increased levels of bPAC lead to Ca2+ transients with longer widths. C) Increasing bPAC leads to increased time between events.

Supplemental Data

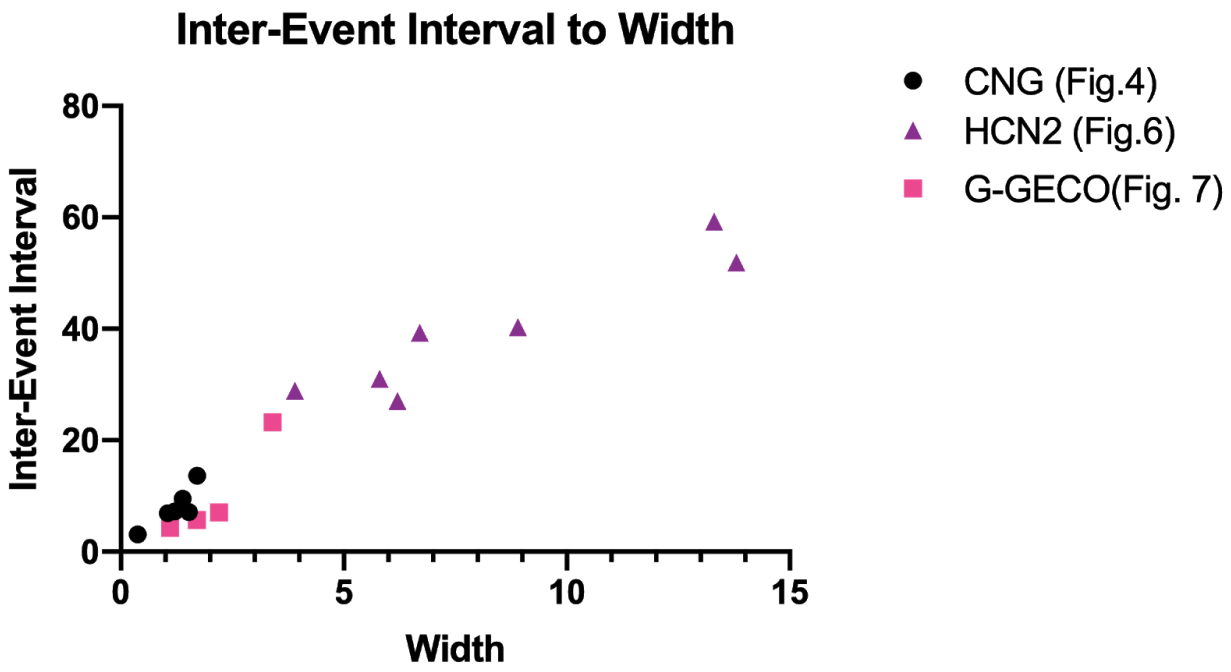

Supplemental Figure 1 : Inter-Event Intervals are linearly dependent on the event width.